SPITZER OBSERVATIONS OF THE λ ORIONIS CLUSTER. II. DISKS AROUND SOLAR-TYPE AND LOW-MASS STARS

JESÚS HERNÁNDEZ[1], MARIA MORALES-CALDERON[2], NURIA CALVET[3], L. HARTMANN[3], J. MUZEROLLE[4], R. GUTERMUTH[5,6], K. L. LUHMAN[7], AND J. STAUFFER[8]

[1] Centro de Investigaciones de Astronomía, Apdo. Postal 264, Mérida 5101-A, Venezuela; hernandj@cida.ve
[2] Laboratorio de Astrofisica Estelar y Exoplanetas (LAEX), Centro de Astrobiologia (CAB, INTA-CSIC), LAEFF, P.O. Box 78, E-28691, Villanueva de la canada, Madrid, Spain
[3] Department of Astronomy, University of Michigan, 830 Dennison Building, 500 Church Street, Ann Arbor, MI 48109, USA
[4] Space Telescope Science Institute, 3700 San Martin Drive, Baltimore, MD 21218, USA; muzerol@stsci.edu
[5] Five Colleges Astronomy Department, Smith College, Northampton, MA 01027, USA
[6] Department of Astronomy, University of Massachusetts, Amherst, MA 01003, USA
[7] Center for Exoplanets and Habitable Worlds, The Pennsylvania State University, University Park, PA 16802, USA
[8] Spitzer Science Center, Caltech M/S 220-6, 1200 East California Boulevard, Pasadena, CA 91125, USA

ABSTRACT

We present IRAC/MIPS *Spitzer Space Telescope* observations of the solar-type and the low-mass stellar population of the young (∼5 Myr) λ Orionis cluster. Combining optical and Two Micron All Sky Survey photometry, we identify 436 stars as probable members of the cluster. Given the distance (450 pc) and the age of the cluster, our sample ranges in mass from 2 $M_\odot$ to objects below the substellar limit. With the addition of the *Spitzer* mid-infrared data, we have identified 49 stars bearing disks in the stellar cluster. Using spectral energy distribution slopes, we place objects in several classes: non-excess stars (diskless), stars with optically thick disks, stars with "evolved disks" (with smaller excesses than optically thick disk systems), and "transitional disk" candidates (in which the inner disk is partially or fully cleared). The disk fraction depends on the stellar mass, ranging from ∼6% for K-type stars ($R_C - J < 2$) to ∼27% for stars with spectral-type M5 or later ($R_C - J > 4$). We confirm the dependence of disk fraction on stellar mass in this age range found in other studies. Regarding clustering levels, the overall fraction of disks in the λ Orionis cluster is similar to those reported in other stellar groups with ages normally quoted as ∼5 Myr.

Key words: infrared: stars – open clusters and associations: individual (λ Orionis Cluster) – protoplanetary disks – stars: formation – stars: pre-main sequence

*Online-only material:* color figures, machine-readable tables

1. INTRODUCTION

Circumstellar disks, which appear to be a natural byproduct of the process of star formation, play a critical role in the evolution of stars and planetary systems. As these disks evolve, the rate of accretion onto the central star decreases and the gas dissipates, while some of the remaining dust is thought to coalesce into large bodies such as planets and planetesimals. The more crucial processes in the evolution from primordial disks (e.g., optically thick disks with modest dust coalescence) to planetary systems occur in the age range ∼1–10 Myr, when the dust and gas in the disk is removed (Calvet et al. 2005), second-generation dust is created by collisional cascade (Hernandez et al. 2006; Currie et al. 2008), and planets are expected to form (Podosek & Cassen 1994). Studies with the *Spitzer Space Telescope* (Werner et al. 2004) of the disk evolution of young, low-mass (≤2 $M_\odot$) pre-main-sequence stars (T Tauri stars; TTS) in star-forming regions indicate that at 5 Myr about 80% of primordial disks have dissipated (Carpenter et al. 2006; Dahm & Hillenbrand 2007; Hernandez et al. 2007a, 2008) in agreement with results using near-infrared (NIR) observations (Haisch et al. 2001; Hillenbrand 2005). The disk infrared emission observed in stars bearing primordial disks also declines with age (Hernandez et al. 2007b), suggesting that as time passes, dust grains in the disk collide, stick together, grow to sizes much larger than the wavelength of observation, and settle toward the midplane, which reduces the flaring of the disk and thus the amount of energy radiated (Kenyon & Hartmann 1987; Dullemond & Dominik 2005; D'Alessio et al. 2006). Finally, ∼5 Myr is

the age at which observations (e.g., Hernandez et al. 2009) and models (e.g., Kenyon & Bromley 2004, 2008) suggest that second-generation disks, which may trace active planet formation (Greenberg et al. 1978; Backman & Paresce 1993; Kenyon & Bromley 2008; Wyatt 2008; Cieza 2008), start to dominate the disk population around intermediate-mass stars.

The λ Orionis star-forming region is one of the most prominent OB associations in Orion. It includes a ring-like structure of dust and gas of 8°–10° in diameter (e.g., Maddalena & Morris 1987; Zhang et al. 1989; Dolan & Mathieu 2002). Several young stellar regions are located near the ring (e.g., B30, B35, LDN1588, LDN1603) in which low-mass star formation continues today (Barrado y Navascués et al. 2007a; Mathieu 2008; Morales-Calderon 2009). The λ Orionis cluster (also known as Collinder 69) is located in a region nearly devoid of dense gas near the center of the ring. According to several authors (Maddalena & Morris 1987; Cunha & Smith 1996; Dolan & Mathieu 1999, 2002), λ Orionis (spectral-type O8 III) had a massive companion that became a supernova (SN), removing nearby molecular gas at the center of the cluster about 1 Myr ago. The ring of dust and gas is then the current location of the swept up material from the SN (e.g., Mathieu 2008; Morales-Calderon 2009).

Because the λ Orionis cluster is reasonably nearby (450 pc; see Mathieu 2008) and relatively populous, it represents a valuable laboratory for studies of disk evolution, making statistically significant studies of disk properties in a wide range of stellar masses. Its age of 4–6 Myr (e.g., Murdin & Penston 1977; Dolan & Mathieu 2001) represents an intermediate evolutionary stage
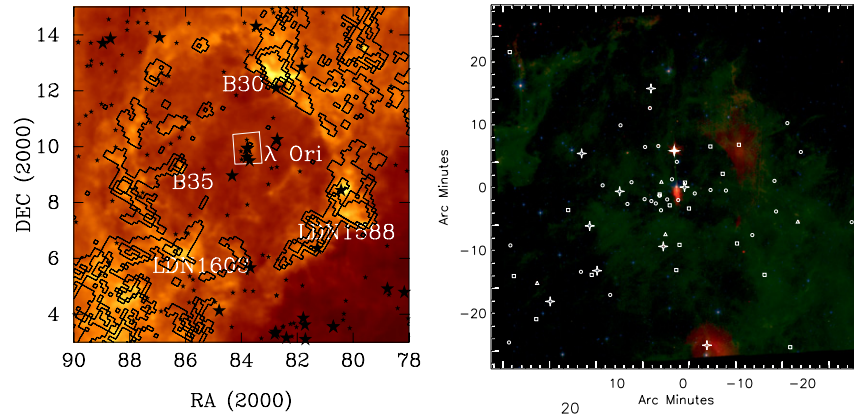
Figure 1. Left panel shows the map of dust infrared emission (Schlegel et al. 1998) of the λ Orionis star-forming region, with superimposed CO isocontours (Dame et al. 2001). Using spectral types in Kharchenko & Roeser (2009), high-mass stars with spectral type earlier than B5 are represented as large stars, while B-type stars with spectral-type B5 or later are represented as small stars. The central box shows approximately the IRAC field studied in this work. The right panel is a false color image of the λ Orionis cluster. It is a three-color composite of IRAC images, 3.6 μm (blue) and 8.0 μm (green), and MIPS image, 24 μm (red). The plot is centered at λ Orionis. We show the location of stars bearing disks. Different symbols represent different types of disks classified in Section 4: circles, squares, and triangles represent thick disks, evolved disks, and pre-transitional and transitional disks, respectively. Intermediate-mass candidates surrounded by debris disks selected in Paper I are represented as open four-point stars. The solid four-point star indicates the Herbig Ae star HD 245185.

(A color version of this figure is available in the online journal.)

between two populous stellar clusters located at similar distances in the Orion star formation complex (Bally 2008) and studied using similar methods to detect and characterize their disks: the σ Orionis cluster (∼3 Myr; Hernandez et al. 2007a) and the 25 Orionis aggregate (7–10 Myr; Hernandez et al. 2007b; Briceño et al. 2007).

The *Spitzer Space Telescope* with its unprecedented sensitivity and spatial resolution in the near- and mid-infrared windows is a powerful tool to expand significantly our understanding of star and planet formation processes; it provides resolved near- and mid-infrared photometry for young stellar populations down to relatively low masses. In a previous paper (Hernandez et al. 2009, hereafter Paper I), we studied the disk population around intermediate-mass stars with spectral types F and earlier in the λ Orionis cluster. In this contribution, we complete a census of the disk population in the cluster studying the infrared excesses produced by disks around stars ranging in mass from solar-type stars to the substellar limit. This paper is organized as follows. In Section 2, we describe the observational data in the cluster. In Section 3, we describe the selection of possible members. In Section 4, we present the method for identifying stars with infrared excesses and the classification of the disk population. In Section 5, we present the disk frequencies of the cluster and we compare these frequencies with results from other stellar groups. Finally, we present our conclusions in Section 6.

2. OBSERVATIONS

2.1. Spitzer Observations

We are using the *Spitzer Space Telescope* observations from Paper I, which include images from the Infrared Array Camera (IRAC; Fazio et al. 2004) with its four photometric channels (3.6, 4.5, 5.8, and 8.0 μm) and from the 24 μm band of the Multiband Imaging Spectrometer for *Spitzer* (MIPS; Rieke et al. 2004).

The region with the complete IRAC data set (hereafter IRAC region) has a size of ∼57′.6 × 54′.6 centered at λ Orionis. More than 40,000 sources were detected in at least one IRAC band using PhotVis (version 1.09), an IDL GUI-based photometry visualization tool developed by R. Gutermuth using the DAOPHOT

modules ported to IDL as part of the IDL Astronomy User Library (Landsman 1993). Final IRAC photometric errors include the uncertainties in the zero-point magnitudes (∼0.02 mag). MIPS observations cover more than 99% of the IRAC region. The absolute flux calibration uncertainty is ∼4% (Engelbracht et al. 2007). Our final flux measurements at 24 μm are complete down to about 0.8 mJy. The detailed description of the observation, reduction, and calibration of the IRAC and MIPS images is given in Paper I.

Figure 1 illustrates the location of the IRAC region (left panel), overlaid on a map of dust infrared emission (Schlegel et al. 1998) and CO isocontours (Dame et al. 2001). The space distribution of disk-bearing stars of the λ Orionis cluster (see Section 4) is shown on a false color image (right panel).

2.2. Optical and Near-IR Photometry

We primarily used the $V R_C I_C$ photometry from Dolan & Mathieu (2002, hereafter DM02) to identify possible members in the λ Orionis cluster. These data were obtained at the Kitt Peak National Observatory using the Mosaic imager on the 0.9 m telescope covering an area of 60 deg² centered in the λ Orionis cluster. Most of the objects in this catalog have magnitudes ranging from $V \sim 10$ to $V \sim 19$. We augmented the optical data set to include the R_C and I_C photometry of 111 very low mass stars and brown dwarfs studied by Barrado y Navascués et al. (2007b, hereafter BN07) not cataloged by DM02. Since there are systematic differences between the R_C and I_C magnitudes of DM02 and BN07 catalogs, we converted the BN07 photometry to the DM02 photometric system. We fitted a straight line in a magnitude–magnitude plot using stars included in both catalogs to obtain the conversion factors needed for each filter.

We combined the optical data set with photometry at J, H, and K_S from the Two Micron All Sky Survey (2MASS) Point Source Catalog (Skrutskie et al. 2006). Out of 5168 optical sources in the IRAC region, 4966 stars (96.1%) have 2MASS counterparts and 21 additional sources have NIR photometry from BN07. About 2752 sources in the 2MASS catalog located in the IRAC region do not have optical information. In general, sources in this sample are below the optical detection limit. In the Appendix,

Table 1
Compiled Membership Information of the λ Orionis Cluster

ID	R.A.(2000) (deg)	Decl.(2000) (deg)	Name(s)	Spectral Type	Ref. (SpT)	Radial Vel. (km s^{-1})	Ref. (r.v.)	Li I (Present)	Ref. (Li I)	Membership Reference	Membership Flag
(1)	(2)	(3)	(4)	(5)	(6)	(7)	(8)	(9)	(10)	(11)	(12)
936	83.43113	9.75636	LOri138	. . .	. . .	. . .	. . .	. . .	. . .	2a	m5
1048	83.44671	9.92733	DM1, LOri001	. . .	. . .	22.44	1	Y	1	1a, 2a	m1
1079	83.44962	10.02767	LOri113	M5.5	2	. . .	. . .	. . .	. . .	2a	m4
1152	83.45800	9.84353	DM2, LOri038	. . .	. . .	24.03	1	Y	1	1a, 2a	m1
1213	83.46550	9.63928	DM3	. . .	. . .	21.27	1	Y	1	1a	m1
1276	83.47354	9.71900	LOri005	. . .	. . .	. . .	. . .	. . .	. . .	2a	m5
1346	83.48471	9.89911	DM4, LOri013	. . .	. . .	2.40	1	Y	1	1b, 2a	m3
1359	83.48587	10.10414	LOri081	M5.5	2	. . .	. . .	. . .	. . .	2a	m4
1531	83.50838	9.68503	DM5	. . .	. . .	28.98	1	Y	1	1a	m1
1728	83.53496	9.85703	LOri044	. . .	. . .	6.52	3	. . .	. . .	2a, 3b	nm2
1733	83.53554	9.84542	LOri109	M5.5	2	28.10	3	. . .	. . .	2a, 3a	m2
1829	83.54658	9.85833	LOri127	. . .	. . .	. . .	. . .	. . .	. . .	2d	nm1
1835	83.54704	9.74078	LOri152	. . .	. . .	. . .	. . .	. . .	. . .	2c	nm1
1840	83.54754	9.70219	LOri072	. . .	. . .	. . .	. . .	. . .	. . .	2a	m5
1844	83.54825	9.82083	LOri086	. . .	. . .	30.01	3	. . .	. . .	2a, 3a	m2
1847	83.54904	9.95092	LOri052	. . .	. . .	36.31	3	. . .	. . .	2a, 3b	nm2
1926	83.55933	9.80731	LOri124-125	M5.5	2	30.76	3	. . .	. . .	2a, 3a	m2
7971	83.90367	9.74011	LOri170	. . .	. . .	. . .	. . .	. . .	. . .	2c	nm1

Notes.

[1] Column 11: (1a) and (1b) represent stars with Li I in absorption from Dolan & Mathieu (2001) and radial velocity in the members range and out of the member range, respectively; (2a), (2b), (2c), and (2d) represent the member flags Y, Y?, N?, and N, respectively, from Barrado y Navascués et al. (2007b); (3a) represents members; (3b) non-members from the radial velocity analysis of Maxted et al. (2008); (4a) and (4b) represent members and non-members from the Li I and radial velocity analysis of Sacco et al. (2008).

[2] Column 12: (m1) represents radial velocity members with Li I in absorption; (m2) represents radial velocity members with no Li I information; m3: represents stars with Li I in absorption and radial velocity out of the member range; (m4) represents both spectral-type and photometric data in agreement with cluster sequence; (m5) represents photometric members; (nm1) represents non-members based on photometric analysis; (nm2) represents non-members based on spectroscopic analysis.

References. (1) Dolan & Mathieu 2001; (2) Barrado y Navascués et al. 2007b; (3) Maxted et al. 2008; (4) Sacco et al. 2008.

(This table is available in its entirety in a machine-readable form in the online journal. A portion is shown here for guidance regarding its form and content.)

we present an IRAC/MIPS analysis for this sample to search for sources with infrared excesses.

3. MEMBERSHIP SELECTION

3.1. Compilation of Known Members

The λ Orionis star-forming region has been the subject of several studies intended to identify members of its stellar and substellar population and some of these overlap with our IRAC region. Duerr et al. (1982) surveyed a region of ~100 deg^2 around λ Orionis identifying nearly 100 Hα emission objects (they used an objective-prism survey). However, most of these objects are located outside the central region, and only two of these objects are in the IRAC region (1624 and 4407). Dolan & Mathieu (2001, 1999) identified 266 pre-main-sequence stars in the λ Orionis star-forming region using the presence of Li I λ6708 in absorption and radial velocities. They reported a mean radial velocity of 24.5 km s^{-1} with small dispersion of radial velocities (2.3 km s^{-1}). Of the 64 sources with Li I in absorption that we have in common with the Dolan & Mathieu (2001, 1999) catalogs (the remaining sources are located outside of IRAC region), four stars have radial velocities outside of the 3σ range (17.6–31.4 km s^{-1}) that Dolan & Mathieu used for identifying members of the cluster. Since these stars have Li I in absorption (a diagnostic of youth) and binaries can lie off the cluster velocity (e.g., Tobin et al. 2009), we placed them as binaries candidates of the λ Orionis cluster.

Using optical and NIR photometry and low-resolution spectroscopy, Barrado y Navascués et al. (2004) reported memberships for 170 low-mass stars and brown dwarf candidates belonging to the λ Orionis cluster. This study was improved by BN07 using new deep NIR photometry, IRAC photometry, and additional low-resolution spectroscopic data. They reported 19 probable non-members, four stars with dubious membership, and 147 bona fide members of the cluster (hereafter BN07 members), of which more than half have spectroscopic measurements of Hα and/or spectral types. All of the BN07 members are in the IRAC region. We revisited the disk population of these objects using methods consistent with previous studies of a number of star-forming regions (Hernandez et al. 2007a, 2007b, 2008), including a better estimation of the effects of errors, for better comparison of disk properties as a function of age and environment (see Section 4).

Recently, Maxted et al. (2008) and Sacco et al. (2008) studied sub-samples of the BN07 members using high-resolution Fiber Large Array Multi-Element Spectrograph (FLAMES; Pasquini et al. 2002) spectra. Based on radial velocity measurements, Maxted et al. (2008) confirmed 69 BN07 members and rejected four using a radial velocity range for members of 22–32 km s^{-1}. Combining three independent criteria including the radial velocity distribution, the presence of the Li I λ6708 line and the Hα line, Sacco et al. (2008) reported membership for 44 BN07 members and five stars confirmed as members of the cluster by Dolan & Mathieu (2001). Since Sacco et al. (2008) did not
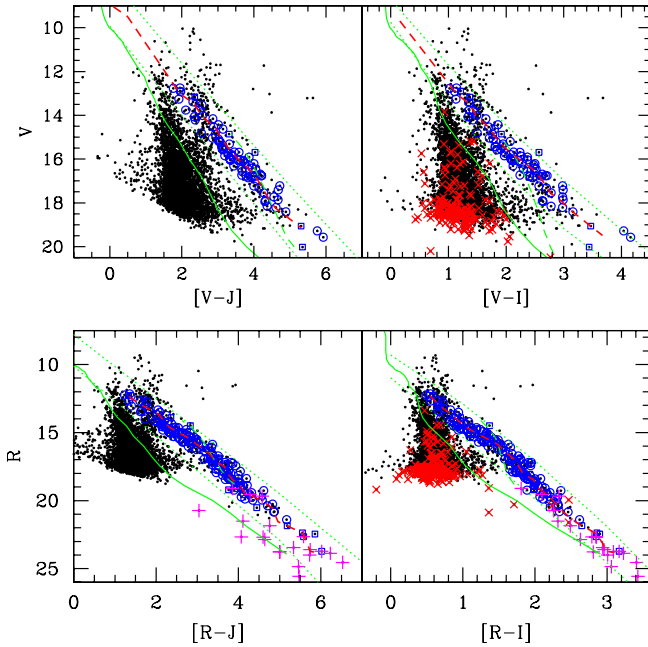
Figure 2. CMDs illustrating the selection of stars in the λ Orionis cluster (λ Ori sample = known members + new photometric candidates). Open circles represent members confirmed using the presence of Li I or radial velocity analysis. Open squares represent other members selected using spectroscopic data (see Table 1). Sources without NIR counterpart are represented with "×" symbols. Sources with NIR photometry from BN07 are represented by crosses. Dashed lines represent the median of colors of the known members in bins of 1 mag in the *V* band (upper panels) or in the *R* band (lower panels). Dotted lines limit the region where members are expected to fall (member regions). These member regions were created using distributions of the known members in each diagram. Assuming a distance of 450 pc, the zero-age main sequence (ZAMS; solid line) was plotted in each panel.

(A color version of this figure is available in the online journal.)

detect Li I in absorption for four BN07 members, they reported them as non-members of the cluster.

Table 1 summarizes the compiled membership information. Column 1 shows the internal running identification number in our sample; Columns 2 and 3 provide the stellar coordinates; Column 4 shows other names used previously; Columns 5 and 6 show spectral types and their references; Columns 7 and 8 show radial velocity measurements and their references, Columns 9 and 10 indicate whether the star has Li I in absorption and their references, respectively. Column 11 shows membership information compiled from previous studies. Based on Column 11, we split the sample of Table 1 in several groups labeled in Column 12: (m1) represents confirmed members of the cluster with Li I in absorption and radial velocity in the member range; (m2) represents stars with radial velocity in the member range but no information about Li I (radial velocity members); (m3) represents stars with Li I in absorption and radial velocity out of the member range (binaries candidates); (m4) represents stars with spectral types and photometric data in agreement with the expected trend in color–magnitude diagrams (CMDs; spectral-type members); (m5) represents known members based only on photometric criteria (photometric known candidates); (nm1) represents non-members based on photometric criteria, and (nm2) represents non-members based on spectroscopic analysis.

3.2. Photometric Selection

To select additional candidates to the ones described in Section 3.1, we used photometric criteria based on their optical-2MASS colors and magnitudes. Figure 2 shows several CMDs

illustrating our photometric selection. First, we estimated empirical isochrones using the location of confirmed members (open circles) and other members selected using spectroscopic criteria (e.g., open squares; radial velocity members, binaries candidates, and spectral-type members) on these CMDs (hereafter confirmed members, radial velocity members, binaries candidates, and spectral-type members are named as "known members" to distinguish from photometric known candidates which are not used in this procedure). Empirical isochrones (dashed lines) were estimated using the median colors ($V - J$, $V - I_C$, $R_C - J$, and $R_C - I_C$) of the known members for 1 mag bins in the *V* band (upper panels) or in the R_C band (bottom panels). Standard deviations (σ) were calculated using the differences between the observed colors of the known members and the expected colors from the empirical isochrones. In each CMD, we fitted two lines using a second order polynomial corresponding to the points representing by the median color + 2.5σ and by the median color—2.5σ, respectively (dotted lines); the regions of probable members are defined between these lines.

Out of 5168 sources with optical photometry within the IRAC region, 4430 sources (∼86%) are likely background sources since they are located below the regions of probable members in all CMDs. We also found 24 foreground candidates located above the regions of probable members in all CMDs. In the right panels of Figure 2, we plotted stars with no 2MASS counterparts (symbol ×). Stars brighter than the magnitude limit in DM02 catalog ($V \sim 20$, $R \sim 18.7$) with no 2MASS counterpart are located below the regions of probable members and thus are likely background stars (220 sources). Stars fainter than the Dolan's photometric limit were taken from BN07, in which most of them have NIR photometry from deeper images. All of BN07 members are located in the regions of probable members in the lower panels of Figure 2 (they are not *V*-band magnitudes for the faintest BN07 members).

Our final sample of candidates of the λ Orionis cluster includes 340 stars located in the regions of probable members in at least three of the four CMDs (297 are located in the four member regions). Additionally, we included 96 stars from BN07 located in the member regions in the lower panels of Figure 2. This sample of 436 stars (hereafter λ Ori sample) includes 150 known members and 32 photometric known candidates. Since a giant branch crosses the empirical isochrones at $V - J \sim 2.5$, $V - I_C \sim 1.5$, $R_C - J \sim 1.8$, and $R_C - I_C \sim 0.7$, large contamination by non-members of the cluster are expected around these colors.

Table 2 shows IRAC and MIPS photometry for the λ Ori sample. Column 1 shows the internal running identification number; Column 2 provides the 2MASS object name; Columns 3 and 4 provide the stellar coordinates; Columns 5, 6, 7, and 8 give the IRAC magnitudes in the bands [3.6], [4.5], [5.8], and [8.0], respectively; Column 9 gives the flux at 24 μm (MIPS band); Column 10 shows the disk classification obtained in Section 4; Column 11 shows references for stars studied previously.

Finally, a group of 77 sources are located in the region of probable members in one or two CMDs but appear as likely foreground or background sources in the other CMDs. Infrared properties of these stars with uncertain photometric membership classification are also studied in the Appendix.

4. DISK POPULATION

To characterize the disk population in the λ Orionis cluster, we need to identify stars in the λ Ori sample (see Section 3.2)

Table 2
Photometric Candidates of the λ Orionis Cluster

ID	2MASS	R.A.(2000) (deg)	Decl.(2000) (deg)	[3.6] (mag)	[4.5] (mag)	[5.8] (mag)	[8.0] (mag)	Flux$_{24\,\mu m}$ (mJy)	Disk Type	Membership Reference[8]
(1)	(2)	(3)	(4)	(5)	(6)	(7)	(8)	(9)	(10)	(11)
30	05331224+0934464	83.30102	9.57958	10.71 ± 0.02	10.71 ± 0.02	10.68 ± 0.02	10.65 ± 0.02	−99.99 ± 99.990	Diskless	...
42	05331308+0937597	83.30452	9.63328	11.50 ± 0.02	11.52 ± 0.02	11.43 ± 0.03	11.45 ± 0.03	−99.99 ± 99.990	Diskless	...
65	05331515+0950301	83.31313	9.84172	11.45 ± 0.02	11.24 ± 0.02	11.08 ± 0.03	10.64 ± 0.02	3.96 ± 0.890	Ev/Thk	...
208	05332084+0958048	83.33684	9.96803	11.69 ± 0.02	11.73 ± 0.02	11.63 ± 0.03	11.63 ± 0.03	−99.99 ± 99.990	Diskless	...
296	05332402+1019535	83.35012	10.33153	10.78 ± 0.02	10.75 ± 0.02	10.81 ± 0.02	10.77 ± 0.02	−99.99 ± 99.990	Diskless	...
328	05332480+1012116	83.35334	10.20324	10.30 ± 0.02	10.26 ± 0.02	10.22 ± 0.02	10.20 ± 0.02	−99.99 ± 99.990	Diskless	...
623	05333353+0935494	83.38974	9.59708	10.44 ± 0.02	10.43 ± 0.02	10.46 ± 0.02	10.42 ± 0.02	−99.99 ± 99.990	Diskless	...
630	05333378+1009233	83.39077	10.15650	10.73 ± 0.02	10.78 ± 0.02	10.76 ± 0.02	10.62 ± 0.02	−99.99 ± 99.990	Diskless	...
7662	05370084+0949045	84.25352	9.81792	9.94 ± 0.02	9.93 ± 0.02	9.87 ± 0.02	9.88 ± 0.02	−99.99 ± 99.990	Diskless	...
7689	05370204+1014447	84.25851	10.24577	11.07 ± 0.02	11.12 ± 0.02	11.10 ± 0.03	11.11 ± 0.03	−99.99 ± 99.990	Diskless	...
7701	05370265+1003583	84.26104	10.06620	11.49 ± 0.02	11.52 ± 0.02	11.47 ± 0.03	11.52 ± 0.03	−99.99 ± 99.990	Diskless	...
7957	...	83.65117	9.92561	15.04 ± 0.03	14.76 ± 0.04	14.19 ± 0.13	14.20 ± 0.14	−99.99 ± 99.990	Thk[3,6]	2a
7968	...	83.80912	9.90209	16.08 ± 0.07	15.86 ± 0.08	16.23 ± 0.73	14.64 ± 0.28	−99.99 ± 99.990	Diskless[4]	2a

Notes. Column 10: Thk-star with an optically thick disk; TD: transitional disk candidate; PTD: pre-transitional disk candidate; EV: star with an evolved (flat) disk; diskless-star with no infrared excesses.
[1] Stars with uncertain 24 μm excess.
[2] Stars with uncertain 8 μm excess.
[3] Stars without 24 μm counterpart.
[4] Faint stars with not reliable excesses at 5.8 μm and 8.0 μm.
[5] Star with moderate IR excess at 8.0 μm, but the 24 μm flux is consistent with the photospheric fluxes.
[6] Classified as evolved disk star from the IRAC SED slope.
[7] The star λ Orionis may mask the detection at 24 μm.
[8] See Table 1.

(This table is available in its entirety in a machine-readable form in the online journal. A portion is shown here for guidance regarding its form and content.)

that exhibit excess emission at the IRAC/MIPS bands. For this purpose, we must properly account for uncertainties and biases in the IRAC/MIPS photometry, particularly near the detection limit of these data (Luhman et al. 2008). In a well-populated sample of stars not strongly affected by extinction, the sum of all these uncertainties and biases (Poisson errors, uncertainties in the zero-point magnitudes, location-dependent variations in the calibration, scatter of photospheric colors among cluster members) is reflected in the spread of colors in a given magnitude among the diskless stars of the cluster, which dominate stellar populations older than ∼2–3 Myr (e.g., Haisch et al. 2001; Hillenbrand 2005; Hernandez et al. 2007a, 2008). Since a disk produces greater excess emission above the stellar photosphere at longer wavelengths, we selected the bands at 8 μm and 24 μm to identify and characterize disks in the stellar population of the λ Orionis cluster. First, we identified disk-bearing stars with infrared excesses at 24 μm and 8 μm in Sections 4.1 and 4.2, respectively. In Sections 4.3 and 4.4, we completed our analysis and classification of the disk population of the λ Orionis cluster based on the excess emission levels observed in the IRAC/MIPS bands and their spectral energy distributions (SEDs).

### 4.1. Identifying Stars with 24 μm Excess

Figure 3 illustrates the procedure to identify stars with 24 μm infrared excess above the photospheric level (e.g., Gorlova et al. 2006, 2007; Hernandez et al. 2006, 2007a, 2007b, 2008). The upper panel shows the K−[24] color distribution of stars in the λ Ori sample detected in the MIPS 24 μm image. The distribution of stars with K−[24] < 1.0 can be described by a Gaussian centered at 0.15 with $\sigma = 0.18$. The 3σ boundaries (dotted lines in lower panels) represent the photospheric colors; thus, stars with excesses at 24 μm have colors K−[24] > 0.69.

Since the λ Orionis cluster has low reddening ($A_V \sim 0.4$; Diplas & Savage 1994), the R−J color can be used as a proxy of spectral types. We display the location of the spectral-type sequence, using the standard R−J colors from Kenyon & Hartmann (1995). The NIR colors from Kenyon & Hartmann (1995) were converted into the 2MASS photometric system using the transformations from Carpenter (2001). We extended the standard R−J colors toward later spectral types using members with spectral types M6 or later reported by BN07. The R−J standard colors were estimated averaging the observed R−J color (BN07) in a given bin of spectral types. There are four candidates bearing disks with small excesses at 24 μm (K−[24] < 1.5); three of them have the lower limit of their error bars inside the photospheric region and thus the 24 μm excess of these objects is not completely reliable. We have marked these objects in Table 2 as stars with uncertain 24 μm excess. Two objects have spectral types ∼M6 or later and are probable brown dwarfs bearing optically thick disks (BN07). There are three stars bearing disks with photometric spectral type earlier than K5. Most stars with 24 μm excess (>75%) have excess ratio at 24 μm ($E_{24} = 10^{0.4*(K−[24]+0.15)}$; e.g., Paper I) larger than 22. The lack of M-type stars with photospheric K−[24] colors reflects the limit magnitude of the 24 μm MIPS band.

4.2. Identifying Stars with 8 μm Excess

Figure 4 shows the IRAC SED slope versus the [8.0] mag for stars in the λ Ori sample illustrating the procedure to detect infrared excesses at 8 μm (e.g., Lada et al. 2006; Hernandez et al. 2007a, 2007b, 2008). The IRAC SED slope ($\alpha = d \log[\lambda F_\lambda]/d \log[\lambda]$) is determined from the [3.6]−[8.0] color. The error bars in α are calculated propagating the photometric errors at [3.6] and [8.0]. To determine the photospheric levels, we used the mean error of α ($\bar{\sigma}$) for stars within 0.5 mag
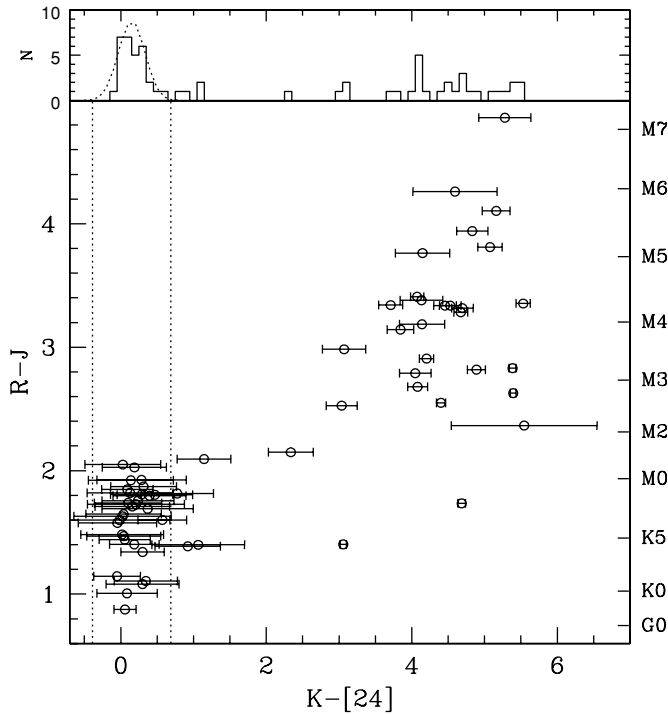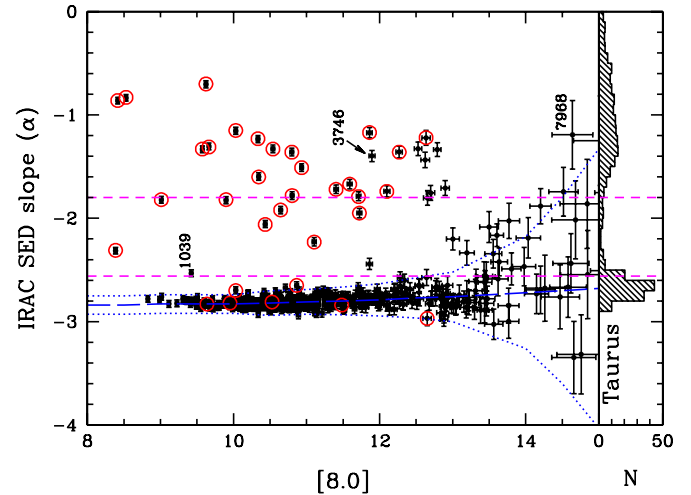
Figure 3. CMD of K−[24] vs. R − J for the λ Ori sample. On the right vertical axis, we show the spectral types that correspond to the standard colors from Kenyon & Hartmann (1995; stars M5 or earlier) and to the typical colors of members from BN07 (stars M6 or later). The upper panel shows the distribution of K−[24] for stars in the λ Ori sample (Section 3.2). Most stars are located at K−[24] ∼ 0.15 exhibiting approximately a Gaussian distribution (dotted line) with σ of 0.18 mag. The 3σ boundaries (dotted lines in lower panels) represent the photospheric region.

Figure 4. IRAC SED slope vs. [8.0] for the λ Ori sample. The slopes were calculated using the [3.6]−[8.0] color. Dotted lines represent the boundaries we have selected for the photospheric colors. The lower dashed line represents the photometric limit used by other authors (e.g., Lada et al. 2006; BN07) to separate stars bearing disks and diskless stars. This limit is not appropriate for the faintest stars in our sample because it does not take into account photometric errors. The upper dashed line represents the limit between thick disks and evolved disk objects from Lada et al. (2006). The right panel shows the IRAC SED slope distribution of the stellar population in Taurus (Luhman et al. 2010). Stars with 24 μm excess (see Figure 3) are represented by points surrounded by large open circles.

(A color version of this figure is available in the online journal.)

bins in the [8.0] band. The photospheric region (dotted lines) is determined using a 3σ̄ criteria from the median values of α (long dashed lines). The width of this region depends on the photometric error of the [8.0] mag, which dominates the uncertainties in α. Thus, a single value of α to separate diskless and disk-bearing stars based on the IRAC color [3.6]−[8.0] is not useful, especially near the IRAC detection limit (Hernandez et al. 2007a). At the faintest [8.0] mag, the photospheric region is too sparsely populated for a reliable measurement of infrared excesses. For instance, star 7968 ([8.0] ∼ 14.5) represents the faintest star with a probable disk based on 8 μm excess. However, since the detections at 5.8 μm and 8.0 μm of this star are background-limited and upward fluctuations of the background noise could contaminate these detections, the presence of a disk around this star needs additional confirmation.

For comparison, short-dashed lines in Figure 4 represent the limits used by BN07 to classify disks around stars in the λ Orionis cluster based on the following criteria (Lada et al. 2006): diskless stars (α < −2.56), optically thick disks (α > −1.8), and optically thin disks (−2.56 < α < −1.8). The criteria used by BN07 is based on the α distribution of the disk population in Taurus (1–2 Myr) from Hartmann et al. (2005), where most of the disk-bearing stars have α > −1.8. The right panel of Figure 4 shows the α distribution of the disk population in Taurus (1–2 Myr) from Luhman et al. (2010) and supports that disk-bearing stars with α < −1.8 are relatively scarce in Taurus and more frequently observed in older stellar regions (Lada et al. 2006; Hernandez et al. 2007a, 2007b, 2008).

In Figure 4, we also display stars with 24 μm excess (open circles) detected in Section 4.1. In general, stars brighter than

[8.0] ∼ 12.0 with significant excesses at 8 μm have excesses at 24 μm. There are some disk-bearing candidates with error bars inside the photospheric region, the 8 μm excess of these objects is uncertain and are identified in Table 2 (see also Section 4.4). Finally, star 1039 is a relatively bright source ([8.0] ∼ 9.5) that shows infrared excess only at 8 μm (>5σ above the photospheric limit). Visual inspection of the image does not reveal any obvious source of contamination at 8 μm. However, at 24 μm (where the disk produces greater excess emission) the star 1039 exhibits photospheric fluxes and thus the presence of a disk around this object is highly uncertain.

4.3. Disk Diagnostics

Figure 5 displays the distribution of disk-bearing stars (with MIPS counterparts) of the λ Ori sample in an SED slope diagram, generated using the K−[5.8] and [8.0]−[24] colors. The K−[5.8] slope represents disk emission at 5.8 μm, while the [8.0]−[24] slope indicates whether the star has a flat (slope ∼ 0) or rising (slope > 0) SED at wavelengths greater than 8 μm. Using colors from Luhman et al. (2010), we display the SED slope distributions (right panel and upper panel) and the quartiles (large error bars) of the disk population in Taurus. The dashed line represents a limit where the inner disk emission has not been affected significantly by evolutionary processes (a lower limit of primordial disks for Taurus; Luhman et al. 2010). About 97% of the disk-bearing stars in Taurus are located above this line. We use this boundary as a proxy to separate stars bearing optically thick disks (above the dashed line) from other types of disks. We show in Figure 5 the location of five transitional disks in several star-forming regions: TW Hya, GM Aur, Coku Tau/4, CS Cha, and CVSO 224 (Calvet et al. 2002, 2005; D'Alessio et al. 2005; Espaillat et al. 2007a, 2008b). Observationally, they are characterized by relatively small excesses at 5.8 μm and large excesses at longer wavelengths. Star 4111 can be identified
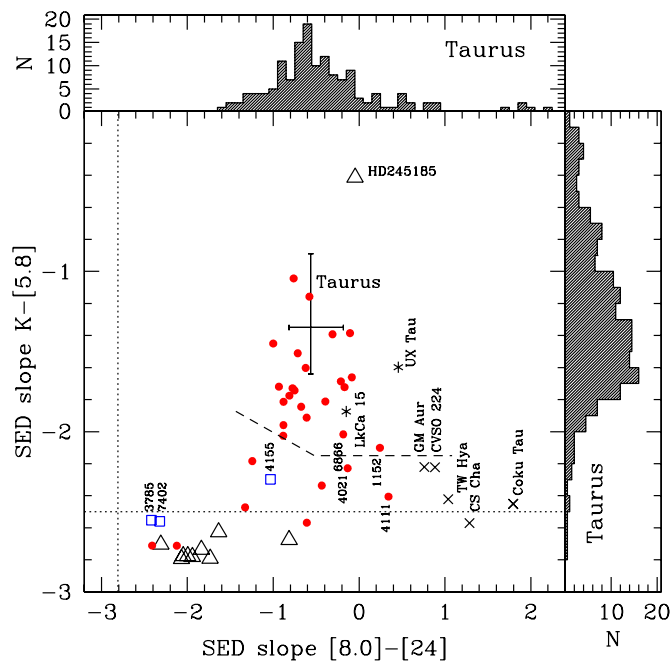
Figure 5. SED slopes from K−[5.8] and [8.0]−[24] for disk-bearing stars of the λ Orionis cluster with photometric spectral types of B–F (triangles; Paper I), G−K4 (squares), and K5 or later (circles). For reference, we display the location of five transitional disk objects (GM Aur, CVSO 224, TW Hya, CS Cha, Coku Tau/4) and that of two pre-transitional disk objects (LCa 15 and UX Tau A). Photospheric limits are indicated with dotted lines. Dashed line represents the lower boundary of primordial disks from Luhman et al. (2010). This line is used as a reference to separate stars bearing optically thick disks from other types of disks: transitional disk candidates (∼below the limit with SED slope [8.0]−[24] > 0), pre-transitional disk candidates (∼below the limit with SED slope [8.0]−[24] ∼ 0), and evolved disk systems (∼below the limit with [8.0]−[24] < 0). Early-type stars below the photospheric limit of K−[5.8] are likely debris disk systems (triangles; Paper I). The right panel and the upper panel show the SED slope distributions from K−[5.8] and [8.0]−[24] for the Taurus disks (Luhman et al. 2010); the error bar represents the median and quartiles for the Taurus disks.

(A color version of this figure is available in the online journal.)

as a transitional disk candidate. Since star 1152 has a rising SED after 8 μm and it is near the optically thick disk limit, we also place this star as a transitional disk candidate. The disk of the star Coku Tau/4 is circumbinary, and its structure is a result of tidal truncation due to the binary orbit (Ireland & Kraus 2008). There is a possibility that our transitional disk candidates can be binary systems and their disks are similar to the disk associated with Coku Tau/4. In addition, Figure 5 shows the location of the newly discovered class of pre-transitional disks (LkCa 15 and UX Tau A), in which gaps in primordial disks rather than holes have been identified (Espaillat et al. 2007b, 2008a; Brown et al. 2008). Two objects (4021 and 6866) have similar [8.0]−[24] color than the pre-transitional disk LkCa 15, but with less infrared excesses at 5.8 μm. We placed these objects as possible pre-transitional disks in the cluster; however, a more detailed study is necessary to reveal the actual nature of their disks.

About 30% of the late-type stars bearing disks in the λ Orionis cluster exhibit relatively small IRAC/MIPS excesses (below the dashed lines and with SED slope [8.0]−[24] < 0) indicating that evolutionary processes (e.g., grain growth, dust sedimentation, and/or settling) have been at work, generating flatter disk structures (D'Alessio et al. 2006; Dullemond et al. 2007; Manoj 2010). We identify these sources as evolved disk

stars in Table 2. We plotted with squares the three earliest stars with infrared excesses (photometric spectral type earlier than K5). One of these stars (4155) exhibits modest infrared excess at 5.8 μm and 24 μm, while the other two stars (3785 and 7402) exhibit marginal infrared excesses at 24 μm and no excesses at 5.8 μm. For comparison, we show the locations of the intermediate-mass stars bearing disks studied in Paper I; except for the Herbig Ae/Be star HD 245185, these are debris disk candidates, with no excesses in the IRAC bands and varying degrees of excesses at 24 μm.

There are 18 disk-bearing candidates with excesses at 8 μm but without MIPS counterparts (see Figure 4). In general, these stars are below the MIPS detection limit. Only star 3746 could be above the MIPS detection limit; however, it is located near the star λ Ori which may mask the detection at 24 μm. The disks around two stars (1039 and 7968) are highly uncertain (see Section 4.2). In summary, based only on the IRAC SED slopes (Section 4.2), we found six stars with optically thick disks, seven evolved disk stars and four stars with uncertain 8 μm excess emission. SEDs of individual objects will be detailed in the following section.

4.4. Spectral Energy Distributions

Figures 6 and 7 show SEDs of the candidates bearing disks with and without MIPS counterparts, respectively. Fluxes calculated from optical magnitudes (BN07, DM02), 2MASS photometry (J, H, K), IRAC bands (3.6, 4.5, 5.8, and 8.0 μm), and the 24 μm MIPS band were normalized to the flux in the J band. We sorted the SEDs by photometric spectral types, which were calculated interpolating the R − J color in the standard color sequence (Kenyon & Hartmann 1995). Since the R − J colors are not corrected by reddening, the photometric spectral type corresponds to a later limit. We display the median SED of the disk population in Taurus. It was constructed from the median colors (2MASS, IRAC, and MIPS) of low-mass stars (with spectral types K and M) bearing disks from Luhman et al. (2010). We also show the photospheric fluxes for a star with the corresponding photometric spectral type (Kenyon & Hartmann 1995) normalized to the J band. To compare our results with those from BN07, we display the IRAC/MIPS photometry given by BN07, with their identification number, disk type, and spectral type (when is available). In general, disk types identified in Section 4.3 agree with those given by BN07. Star 1152 (spectral type M2; thick disk in BN07) shows small or no infrared excesses at wavelengths shorter than 8 μm and infrared excess at 24 μm comparable to stars bearing an optically thick disk; we classified this star as a transitional disk candidate. On the other hand, the star 3597 (spectral type M4; transition disk in BN07) exhibits a decreasing SED after 8 μm. We classified this object as an evolved disk star.

Three disk-bearing stars with photometric spectral types K7 or earlier (3785, 7402, and 1310) have marginal infrared excesses at 24 μm and no excesses detected in the IRAC bands. The disk suggested for these objects needs additional confirmation. If disks are present around these stars, their infrared excesses are comparable to those observed in the early-type debris disk candidates (Paper I) indicating probably a similar origin of their infrared emission (e.g., Gorlova et al. 2007; Kenyon & Bromley 2005). The K-type star 4155 clearly exhibits infrared excesses at 8 μm and moderate excess at 24 μm. The excesses around this star could be explained if the disk is in an intermediate phase evolving from a primordial to a debris disk (evolved disk). The star 5447 was not included
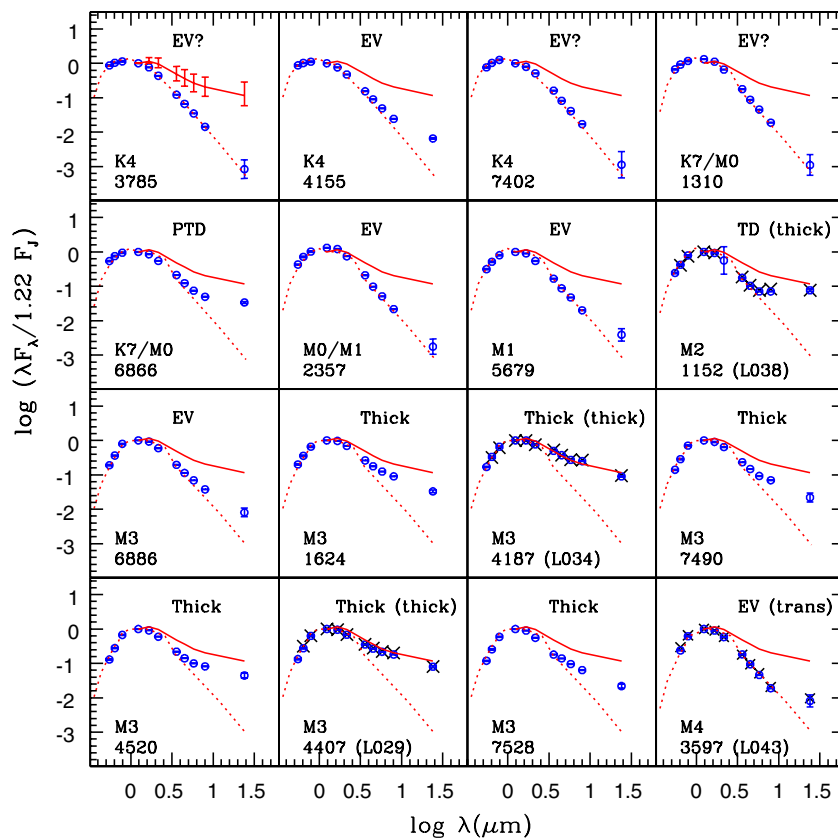
(a)
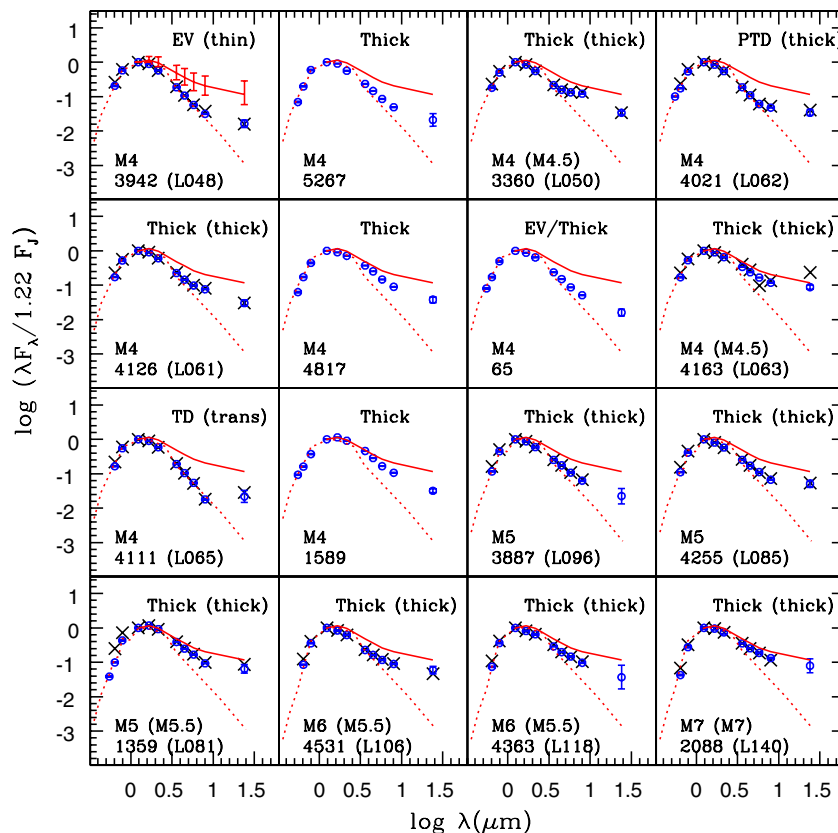
(b)

Figure 6. (a) SEDs for stars in the λ Ori sample with IR excesses and MIPS detections. (b) SEDs for late-type stars with IR excesses and MIPS detections. In each panel, we show our identification number, the photometric spectral type, and the disk type found in Section 4.3. Photometric spectral types are given using the $R - J$ colors and standard calibrations. Dotted lines show the corresponding photospheric levels (Kenyon & Hartmann 1995). For comparison, we show in parentheses the identification number, the spectral type (when available), and the disk type for stars studied by BN07. The photometry from these authors are represented by crosses. We plot the median SED slope of the disk population in Taurus (solid line; Luhman et al. 2010); error bars shown in the first panel denote the corresponding quartiles.

(A color version of this figure is available in the online journal.)
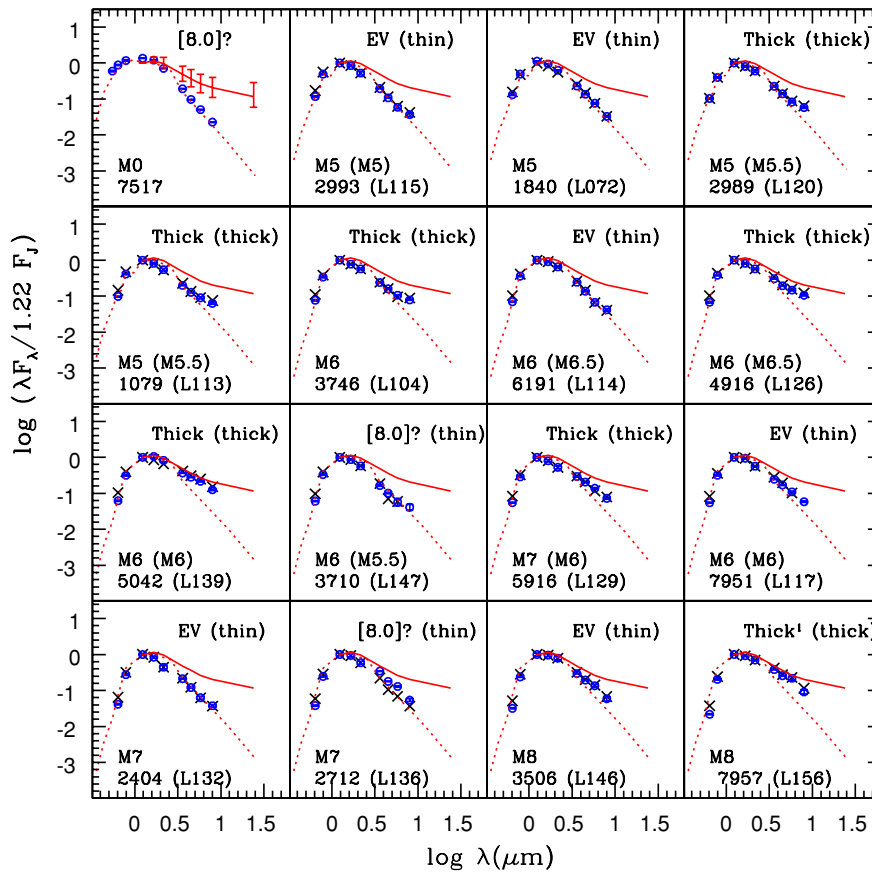
Figure 7. SEDs for late-type stars with IR excesses and without MIPS detections. Symbols and labels are similar to Figure 6. From the IRAC SED slope, star 7957 was classified bearing a thin disk. The SED of this object suggests that 7957 has an optically thick disk.

(A color version of this figure is available in the online journal.)

in Figure 7, the SED of this thick disk object is similar to that observed in the star 7490 (spectral type M4).

In Figure 7, there are three stars (7517, 3710, and 2712 with spectral types M0, M6, and M7, respectively) with marginal infrared excesses at 8 μm which could be produced by either disk emission or polycyclic aromatic hydrocarbon (PAH) contamination. The IRAC photometry of the star 2712 could also be contaminated by a near bright source (located at $\sim 7''$). Based on the IRAC SED slope (Figure 4), the star 7957 is classified as an evolved disk star with a marginal excess at 8 μm. However, the SED observed for this source shows excesses in all IRAC bands similar to those observed in sources with thick disks in agreement with the disk type reported by BN07.

There are 16 stars with a thin disk type in BN07 that we classified as diskless star based on the criteria discussed above. Figure 8 shows SEDs for these objects. Several possibilities may support our diskless classification. Three stars only have photometry in the [3.6], [4.5], and [5.8] bands in BN07. Based on the IRAC SED slope, BN07 classified as disk-bearing stars objects with $\alpha > -2.56$, six of these objects are located in the diskless region in the [3.6]−[4.5] versus [5.8]−[8.0] diagram presented by these authors. As discussed in Section 4.2, the photospheric region of the IRAC slope depends on the brightness of the star and thus the single value of the IRAC SED slope applied by BN07 to separate diskless and disk-bearing stars does not work well, particularly, for the faintest stars. In addition, [8.0] mag given by BN07 are systematically 0.1 mag brighter than our photometry. The K−[8.0] colors of the diskless stars

(with photometric spectral types M5 or earlier) in this work are in good agreement with the standard K−[8.0] colors derived from STAR-PET tool available on the *Spitzer* Science Center Web site.

5. DISK FREQUENCIES AND DISK DIVERSITY OF THE λ ORIONIS CLUSTER

The upper panel in Figure 9 shows disk frequencies as a function of photometric spectral types estimated using the $R_C - J$ color. To reduce the contamination by non-members, frequencies were calculated using the members confirmed by Dolan & Mathieu (2001), BN07, Maxted et al. (2008), and Sacco et al. (2008); see Section 3.1. We plotted the fractions of confirmed members with optically thick disks (filled circles and solid line) and the fractions of confirmed members bearing any type of disks (open squares and dotted line) including evolved disks and pre-transitional/transitional disks. These fractions decrease for decreasing $R_C - J$ color and flatten up around $R_C - J \sim 4.5$ (spectral types M6–M7). The disk fraction may decline toward later spectral types; however, including the error bars, the data are consistent with no change in disk frequency from M6 to later types

For reference, we plot the masses corresponding to the $R_C - J$ colors along the 5 Myr isochrone of Siess et al. (2000). Since $R_C - J$ color bins represent different ranges in stellar masses, the decrease of disk frequencies toward earlier spectral types indicates that primordial disks dissipate faster as the stellar mass
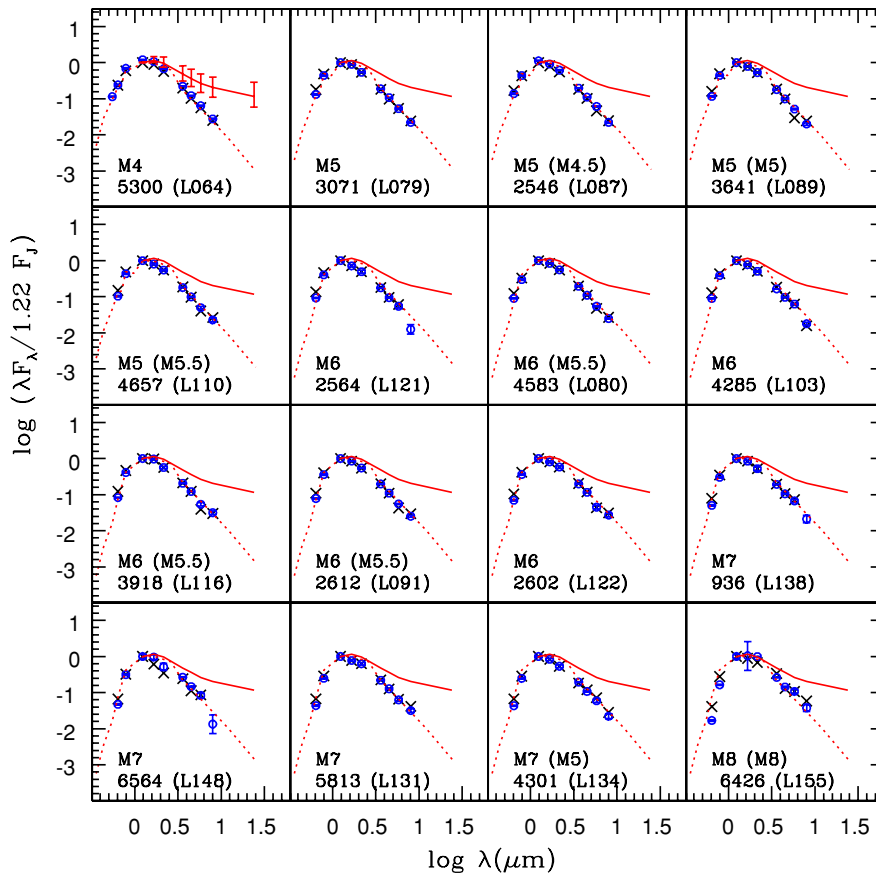
Figure 8. SEDs for diskless stars classified previously as stars bearing thin disks (BN07). Symbols and labels are similar to Figure 6.
(A color version of this figure is available in the online journal.)

increases. Particularly, for solar-type stars the disk frequency is ∼6%, while for very low mass stars and brown dwarf mass range ($M/M_\odot < 0.1$) the disk frequency increases to ∼27%. The decrease of disk frequencies toward higher stellar mass agrees with results in other young stellar populations, e.g, IC 348 (Lada et al. 2006), Upper Scorpius (Carpenter et al. 2006), the σ Ori cluster (Hernandez et al. 2007a), and the Ori OB1b subassociation (Hernandez et al. 2007b). For reference, the lower panel of Figure 9 shows the location on the color–magnitude diagram of stars bearing disks selected in Section 3.2. In general, the disk population of stars with spectral-type M2 or earlier includes evolved disk objects while optically thick disks are more frequently observed at later spectral types.

Using the lower panel of Figure 9, we can estimate the contamination levels in our sample. We calculated disk fractions in several $R_C - J$ color bins for the confirmed members of the λ Orionis cluster (F_{disk}^{mem}) and for the entire λ Ori sample (F_{disk}^{phot}). Assuming that the source of contamination are photometric candidates without infrared excesses and stars with infrared excesses are members of the cluster-bearing disk, we can estimate the contamination level (F_{nomem}) expected in the λ Ori sample applying the relation $F_{nomem} = 1 - F_{disk}^{phot}/F_{disk}^{mem}$. Figure 10 shows the contamination level versus the color $R_C - J$. As discussed in Section 3.2, the larger contamination level is produced by main-sequence stars and by a giant branch that cross the λ Orionis young stellar population at $R_C - J \lesssim 2.5$. In general, the level of contamination for M-type stars is less than 25%.

Regardless of different environments and clustering levels, the overall disk frequency for M-type stars in the λ Orionis cluster (18.5% ± 4.0%) is comparable to those reported in other stellar groups with ages normally quoted as ∼5 Myr. The more dispersed stellar groups, Upper Scorpius (19% ± 4%; Carpenter et al. 2006) and the Orion OB1b subassociation (15% ± 4%; Hernandez et al. 2007b), have disk frequencies similar to that observed in the λ Orionis cluster. This suggests that the clustering levels of stellar groups does not affect significantly the disk frequencies observed at 5 Myr. In particular, the Orion OB1b subassociation and the λ Orionis cluster have similar stellar mass—disk frequency dependencies (see Paper I). The disk frequency for stars later than K5 (stellar mass < 1 $M_\odot$) in the stellar cluster NGC 2362 (5 Myr; Dahm & Hillenbrand 2007) is slightly higher 23.0% ± 3.4%) than that for the λ Orionis cluster. The number of evolved disks may be overestimated by Dahm & Hillenbrand (2007) as they did not correct for larger photometric errors at faint magnitudes (see Section 4). Finally, if the SNe hypothesis proposed by Dolan & Mathieu (1999, 2002) is correct, the similarities in the disk frequencies for several stellar groups suggest that the disk population in the λ Orionis cluster was not affected significantly by the SNe.

The detection of evolved disks and pre-transitional/transitional disk candidates in the cluster supports the existence of at least two different pathways in the evolution from primordial disks to second-generation disks (e.g., Hernandez et al. 2007a; Cieza 2008; Manoj 2010; Currie 2010). Using the M-type stars with MIPS counterparts (Figures 5 and 6),
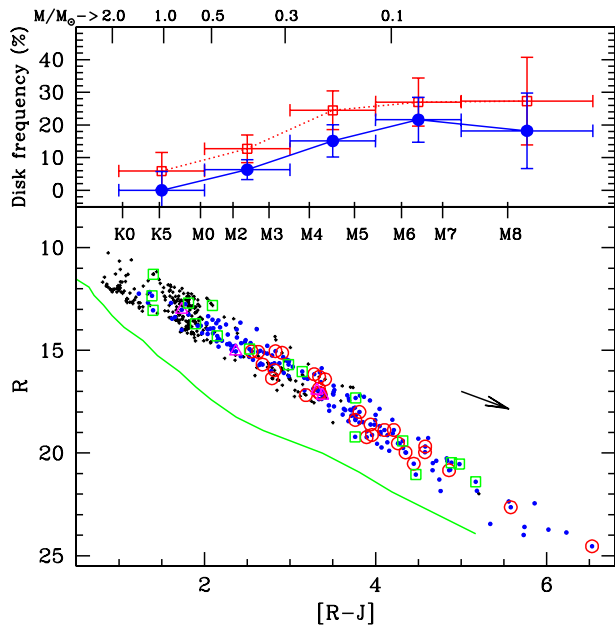
Figure 9. Upper panel: disk frequency as a function of photometric spectral type, estimated using the $R_C - J$ color. The spectral-type scale was calculated using the standard colors from Kenyon & Hartmann (1995) and the typical $R_C - J$ color of members from BN07 with spectral-type M6 or later (see Section 4.1). We display stellar masses using the 5 Myr isochrone from Siess et al. (2000). The disk frequencies for stars bearing optically thick disks (filled circles) and for all disk-bearing stars (open squares) decrease toward higher stellar masses. Lower panel shows the locations of disk-bearing stars of the λ Orionis cluster on a color–magnitude diagram. Members from Dolan & Mathieu (2001), BN07, Sacco et al. (2008), and Maxted et al. (2008) are represented by solid circles; photometric candidates selected in Section 3.2 are represented by small crosses. Different open symbols represent different types of disks found in Sections 4.3 and 4.4; circles, squares, and triangles represent thick disks, evolved disks, and pre-transitional and transitional disks, respectively. The solid line is the ZAMS (Siess et al. 2000) located at 450 pc.

(A color version of this figure is available in the online journal.)

the frequency of pre-transitional/transitional disks in the λ Orionis cluster is 13.3 ± 6.7 (6.7 ± 4.7 for the transitional disk candidates alone), comparable to that observed in other stellar clusters with ages of 3 Myr or older (see Muzerolle et al. 2010). The relative scarcity of transitional disks can be used to indicate that the phase from primordial disks to second-generation disks through "the transitional disk evolutionary pathway" is relatively short. While Sicilia-Aguilar et al. (2008) reported a relatively high fraction (40%–50%) of transitional disks for the Coronet cluster (age ∼ 1 Myr), Ercolano et al. (2009) show that this fraction was overestimated, reporting a transitional disk fraction of ∼15% ± 10% for the cluster. On the other hand, one-third (33.3% ± 10.5%) of the disk population in the λ Orionis cluster is classified as evolved or pre-transitional/transitional disks (hereafter evolved-transitional disks).

Using the same method to classify disk populations, the evolved-transitional disk fractions in the σ Orionis cluster (∼3 Myr), the Orion OB1b subassociation (∼5 Myr), and in the 25 Orionis (8–10 Myr) aggregate are 17.5% ± 5.3%, 35.3% ± 14.4%, and 40.0% ± 20.0%, respectively. In contrast, Currie et al. (2009) reported as many as 80% of evolved-transitional disk fraction for the 5 Myr old cluster NGC 2362. Based on this, they reported that the timescale for disk dissipation is comparable with the median primordial disk lifetime. However, the reported fractions of evolved disks strongly depend on the limit used to separate primordial and
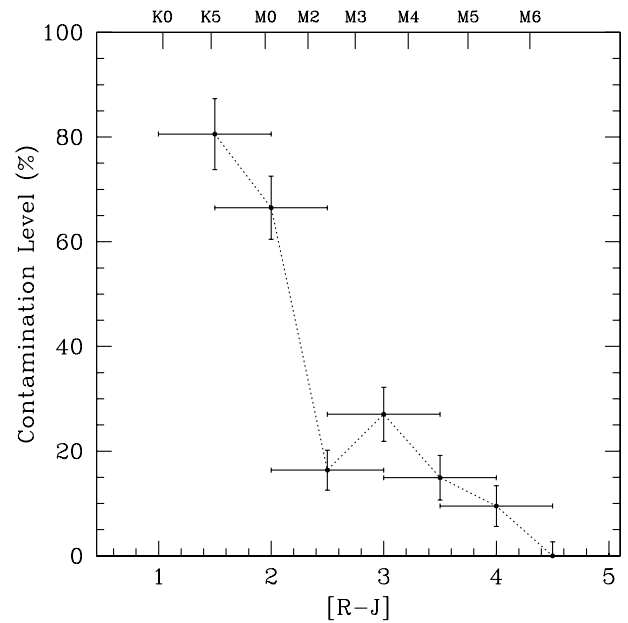
Figure 10. Contamination level as a function of $R_C - J$. To estimate the level of contamination by non-members in the λOri sample (Section 3.2), we calculate disk frequencies in this sample in several bins of colors (F_{disk}^{phot}). The disk frequencies assumed for the λ Orionis cluster (F_{disk}^{mem}) are calculated using the confirmed members from Dolan & Mathieu (2001), BN07, Sacco et al. (2008), and Maxted et al. (2008). The contamination level is $100*(1-F_{disk}^{phot}/F_{disk}^{mem})$.

evolved disks. For instance, Currie et al. (2009) used the lower quartile of the median Taurus SED (Furlan et al. 2006) to classify primordial and evolved disks (∼25% of the disk-bearing stars in Taurus are located below this limit). In Figure 5, we used the boundaries defined by Luhman et al. (2010) which follow the upper edges of the color gaps between diskless stars and stars bearing disks in Taurus. Using this criteria, 97% of the disk-bearing stars in Taurus are classified as primordial disks (statistically this means a limit of $>2\sigma$). Moreover, the disk population in Taurus shows a large dispersion in disk emission (Hartmann et al. 2005; Luhman et al. 2010; Furlan et al. 2006, 2009). This could be a reflection of the initial properties of these disks, of different rates for disk dispersion processes, and/or of different intrinsic properties of the star-disk systems (e.g., multiplicity, mass of the central object, inclination angle of the disk; Manoj 2010; Hillenbrand 2008). Thus, it is difficult to define a reliable criteria to indicate the starting point in the evolution from primordial to second-generation disks and, without an individual detailed modeling, the evolved-transitional disk fractions are reference values that can be used to compare different disk populations assuming an certain criteria. In any event, the observation of more evolved-transitional disks stars (given a certain criteria) in older stellar groups does not necessarily imply longer timescales for evolved-transitional disks. An alternative is that star formation has stopped and there is no steady supply of primordial disks (Manoj 2010). There is also the possibility that the criteria to define primordial disks may be limited and some misclassified evolved disks are still in a primordial disks phase (Luhman et al. 2010; Muzerolle et al. 2010; Manoj 2010).

6. SUMMARY AND CONCLUSIONS

We have used the IRAC and MIPS instruments on board the *Spitzer Space Telescope* to study the disk population of

the λ Orionis cluster. Using optical photometry and members confirmed by spectroscopy, 436 candidates were selected from optical-2MASS CMDs. The level of contamination by non-members depends on the spectral-type range, showing the lowest level of contamination ($\lesssim$25%) for M-type stars. Combining optical, 2MASS, and *Spitzer* data and following the procedure used in previous disk census (Hernandez et al. 2007a, 2007b, 2008), we have reported 49 stars bearing disks, 16 of which were detected only in the IRAC bands. Out of 49 disk-bearing stars, 38 were reported previously as members of the λ Orionis cluster (BN07; Dolan & Mathieu 2001), 11 stars are new members of the cluster based on its infrared excesses and its optical colors and magnitudes.

Based on their SEDs and an SED slope diagram, we classified the disk-bearing stars with MIPS counterpart in three classes: 20 thick disk stars, nine evolved disk stars, two transitional disk candidates, and two pre-transitional disk candidates. We found that for stars with color $R-J > 3$ (~later than M3.5) the disk frequencies are 20%–30%, while stars with colors $R-J < 3$ (~earlier than M3.5) the disk frequencies are <20%. This indicates a mass-dependent timescale for disk dissipation in the λ Orionis cluster, similar to results in other young star populations (Carpenter et al. 2006; Hernandez et al. 2007a, 2007b, 2008; Lada et al. 2006). The overall disk frequency for M-type stars in the λ Orionis cluster (18.5 ± 4.0) is similar to those reported in stellar groups with similar evolutionary stage: the cluster NGC 2362 ($\lesssim$23% ± 3%; Dahm & Hillenbrand 2007), the OB association Upper Scorpius (19% ± 4%; Carpenter et al. 2006) and the Orion OB1b subassociation (15% ± 4%; Hernandez et al. 2007b). This suggests that the clustering level of the stellar group does not affect significantly the disk frequencies observed at 5 Myr. This work combined with Paper I represents a complete disk census of the stellar population in the λ Orionis cluster.

APPENDIX

ADDITIONAL INFRARED EXCESS SOURCES

We looked for additional members with infrared excesses of the λ Orionis cluster analyzing the infrared properties of two samples not included in our photometric selection (Section 3.2): stars with 2MASS photometry without optical information (Section 2.2) and stars with uncertain photometric membership derived from the CMDs (Section 3.2). Out of 2752 2MASS sources in the IRAC region without optical information, 43 sources have detections at 24 μm. Out of 77 sources with uncertain photometric membership, 18 sources have detections
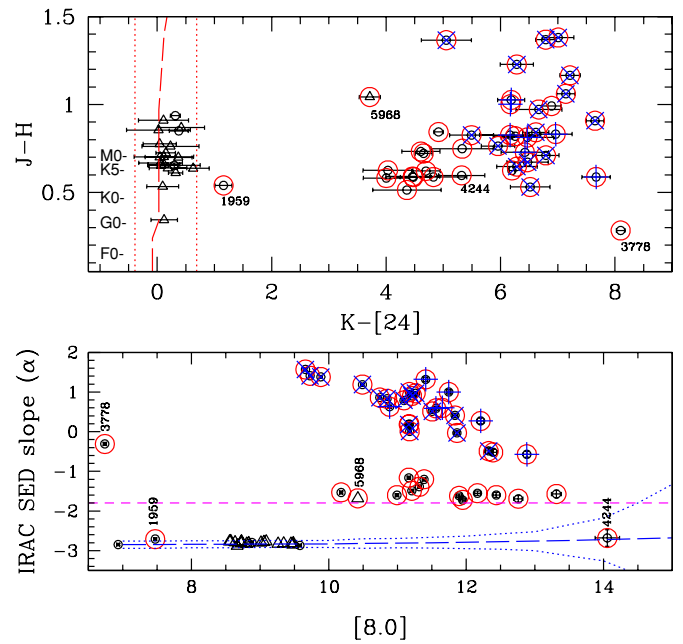
Figure 11. Diagrams used to identify objects with excesses at 24 μm and 8 μm for MIPS sources not included in the λ Ori sample. We plot 2MASS sources without optical photometric (circles) and sources with uncertain photometric membership (triangles). The upper panel shows the color–magnitude diagram K−[24] vs. $J-H$ (see Section 4.1). We display the limits used in Figure 3. The lower panel shows the IRAC SED slope vs. [8.0] diagram K−[24] (see Section 4.2). We display the limits used in Figure 4. Objects surrounded by large circles represent sources with excesses at 24 μm. We show possible galaxies (symbol ×) and other diffuse objects (crosses) selected by visual inspection.

(A color version of this figure is available in the online journal.)

at 24 μm. Following the procedure described in Sections 4.1 and 4.2, Figure 11 shows the diagrams used to identify stars with excesses at 24 μm and 8 μm for these 61 sources with MIPS counterparts. In the upper panel, we have identified 41 sources with excesses at 24 μm. Those sources that do not exhibit excesses at 24 μm do not exhibit excesses at 8 μm (bottom panel). On the other hand, there are two sources (1959 and 4244) that do not exhibit excesses at 8 μm but exhibit excesses at 24 μm. In general, sources with IR excesses are 2MASS objects without optical information, only one (5968) has uncertain photometric membership. This star is located in the regions of probable members in the $V-J$ versus V and the $R_C - J$ versus R_C diagrams, but it appears slightly below from the regions of probable members in the $V - I_C$ versus V and the $R_C - I_C$ versus R_C diagrams.

Visual inspection on the IRAC/MIPS images reveals that most sources with the largest IR excesses are non-stellar. We found that 16 sources are galaxies, and seven sources have slightly larger point-spread function (PSF) widths than other stellar sources on the images (labeled as stellar).

Table 3 shows IRAC/MIPS photometry for the 41 sources with infrared excesses. Column 1 shows the internal running identification number; Column 2 provides the 2MASS object name; Columns 3 and 4 provide the stellar coordinates; Columns 5, 6, 7, and 8 give the IRAC magnitudes in the bands [3.6], [4.5], [5.8], and [8.0], respectively; Column 9 gives the flux at 24 μm (MIPS band); Column 10 shows comments based mainly on the visual inspection on the IRAC/MIPS images. Special notes about some interesting objects are given below Table 3.

Table 3
Additional Sources with Infrared Excesses

ID	2MASS	R.A.(2000) (deg)	Decl.(2000) (deg)	[3.6] (mag)	[4.5] (mag)	[5.8] (mag)	[8.0] (mag)	Flux$_{24\,\mu m}$ (mJy)	Comments
(1)	(2)	(3)	(4)	(5)	(6)	(7)	(8)	(9)	(10)
241	05332198+1002019	83.34160	10.03387	12.928 ± 0.022	12.700 ± 0.023	12.464 ± 0.038	11.949 ± 0.038	1.42 ± 0.85	
336	05332499+0937360	83.35415	9.62667	13.658 ± 0.025	13.439 ± 0.028	13.467 ± 0.082	11.177 ± 0.027	1.89 ± 0.98	Galaxy
387	05332696+1001394	83.36234	10.02764	14.417 ± 0.031	13.833 ± 0.031	13.306 ± 0.068	12.393 ± 0.054	1.87 ± 0.93	
415	05332785+0933527	83.36605	9.56464	14.469 ± 0.030	14.366 ± 0.037	13.560 ± 0.070	11.211 ± 0.027	2.00 ± 0.86	Galaxy
547	05333119+0958575	83.38000	9.98265	14.919 ± 0.034	14.793 ± 0.042	14.491 ± 0.168	12.210 ± 0.049	1.79 ± 0.95	Stellar?
685	05333531+1008261	83.39715	10.14059	14.425 ± 0.029	14.208 ± 0.034	13.938 ± 0.084	13.314 ± 0.073	1.11 ± 0.82	
907	05334256+1003478	83.42737	10.06328	13.812 ± 0.025	13.169 ± 0.025	12.567 ± 0.040	11.172 ± 0.026	5.16 ± 0.85	
1110	05334885+0959544	83.45355	9.99847	14.251 ± 0.029	14.076 ± 0.033	13.710 ± 0.079	11.094 ± 0.030	2.12 ± 0.98	Galaxy
1959	05341507+1019091	83.56283	10.31921	7.599 ± 0.020	7.492 ± 0.020	7.458 ± 0.020	7.472 ± 0.020	9.07 ± 1.60	
2040	05341771+0939224	83.57379	9.65623	12.591 ± 0.022	12.295 ± 0.022	11.936 ± 0.031	11.319 ± 0.028	1.59 ± 0.88	
2191	05342233+1023279	83.59305	10.39108	15.027 ± 0.036	14.506 ± 0.036	14.215 ± 0.114	11.410 ± 0.032	3.08 ± 0.89	Stellar?
2773	05344013+0956435	83.66724	9.94544	13.494 ± 0.024	13.355 ± 0.027	12.472 ± 0.047	9.659 ± 0.022	11.80 ± 1.39	Galaxy
3212	05345260+0955500	83.71918	9.93058	11.323 ± 0.021	10.967 ± 0.021	10.677 ± 0.023	10.179 ± 0.022	9.22 ± 1.02	
3245	05345340+0948500	83.72252	9.81390	13.963 ± 0.026	13.794 ± 0.029	13.382 ± 0.071	10.742 ± 0.025	4.16 ± 1.07	Galaxy
3268	05345389+0946268	83.72455	9.77411	14.546 ± 0.030	14.046 ± 0.032	13.646 ± 0.080	11.561 ± 0.032	5.27 ± 0.82	Stellar?
3323	05345526+0935368	83.73026	9.59357	14.425 ± 0.030	14.036 ± 0.031	13.861 ± 0.098	11.505 ± 0.033	2.24 ± 0.97	Galaxy
3451	05345860+0937287	83.74419	9.62465	14.668 ± 0.030	14.222 ± 0.032	13.861 ± 0.090	11.837 ± 0.037	2.06 ± 0.87	Galaxy
3778	05350816+0955344	83.78401	9.92623	8.945 ± 0.020	8.799 ± 0.021	8.390 ± 0.024	6.738 ± 0.023	3149.89 ± 313.33	
3786	05350835+0935535	83.78479	9.59822	12.968 ± 0.022	12.754 ± 0.023	12.597 ± 0.042	11.896 ± 0.035	1.96 ± 0.84	
3822	05350931+0959112	83.78880	9.98646	13.424 ± 0.024	13.351 ± 0.028	12.466 ± 0.041	9.727 ± 0.022	8.22 ± 1.42	Galaxy
3910	05351190+0951178	83.79960	9.85495	13.795 ± 0.028	13.756 ± 0.033	13.541 ± 0.081	11.164 ± 0.034	1.88 ± 0.64	Galaxy
3933	05351228+0955131	83.80120	9.92033	12.079 ± 0.022	11.719 ± 0.022	11.429 ± 0.028	10.992 ± 0.026	3.17 ± 1.45	
4013	05351511+0943596	83.81300	9.73324	14.648 ± 0.032	14.249 ± 0.036	13.982 ± 0.101	11.653 ± 0.034	2.43 ± 0.88	Stellar?
4057	05351649+0954372	83.81873	9.91034	13.555 ± 0.025	13.356 ± 0.027	12.502 ± 0.039	9.883 ± 0.022	5.43 ± 1.04	Galaxy
4244	05352114+1005584	83.83810	10.09958	14.206 ± 0.027	14.169 ± 0.033	14.065 ± 0.099	14.055 ± 0.179	1.48 ± 0.81	
4321	05352343+0955335	83.84766	9.92599	14.512 ± 0.029	14.199 ± 0.033	13.823 ± 0.097	11.172 ± 0.028	2.49 ± 0.50	Galaxy
4405	05352535+0954476	83.85565	9.91324	12.630 ± 0.022	12.329 ± 0.022	12.008 ± 0.032	11.165 ± 0.026	12.28 ± 0.59	
4527	05352872+0934328	83.86968	9.57579	13.292 ± 0.023	13.098 ± 0.025	12.877 ± 0.048	12.164 ± 0.042	1.32 ± 0.85	
4693	05353347+1002087	83.88948	10.03576	14.380 ± 0.032	13.985 ± 0.033	14.192 ± 0.118	12.327 ± 0.047	0.94 ± 0.54	Galaxy
5045	05354444+0945520	83.93517	9.76446	12.392 ± 0.021	12.133 ± 0.022	11.913 ± 0.030	11.209 ± 0.026	4.40 ± 0.88	
5367	05355400+1003458	83.97500	10.06274	14.576 ± 0.032	14.069 ± 0.033	14.078 ± 0.121	11.263 ± 0.026	3.37 ± 0.92	Galaxy
5541	05355903+1013175	83.99598	10.22153	13.765 ± 0.024	13.527 ± 0.026	13.332 ± 0.064	12.759 ± 0.068	1.06 ± 0.84	
5582	05360034+0956488	84.00143	9.94691	14.045 ± 0.026	13.960 ± 0.030	13.387 ± 0.069	10.849 ± 0.024	2.48 ± 0.87	Galaxy
5968	05361125+0946263	84.04689	9.77397	11.437 ± 0.021	11.045 ± 0.021	10.733 ± 0.023	10.422 ± 0.023	3.35 ± 0.85	
6047	05361360+0930386	84.05668	9.51073	14.862 ± 0.033	14.408 ± 0.034	14.287 ± 0.116	12.883 ± 0.054	1.53 ± 0.83	Stellar?
6638	05363109+0953262	84.12955	9.89062	13.904 ± 0.027	13.739 ± 0.030	13.495 ± 0.068	10.884 ± 0.024	2.95 ± 0.87	Stellar?
6797	05363604+0934545	84.15020	9.58182	13.527 ± 0.024	13.337 ± 0.026	13.110 ± 0.053	12.438 ± 0.048	1.01 ± 0.83	
7039	05364332+0957016	84.18051	9.95045	13.992 ± 0.026	13.785 ± 0.030	13.343 ± 0.058	10.489 ± 0.023	6.50 ± 1.01	Galaxy
7179	05364695+0933541	84.19565	9.56505	15.090 ± 0.034	14.993 ± 0.048	14.735 ± 0.195	11.747 ± 0.031	1.25 ± 0.83	Stellar?
7251	05364890+0955423	84.20378	9.92844	12.817 ± 0.022	12.534 ± 0.023	12.179 ± 0.034	11.387 ± 0.028	2.61 ± 0.88	
7615	05365897+0956307	84.24572	9.94187	14.314 ± 0.029	14.053 ± 0.034	13.940 ± 0.099	11.866 ± 0.038	1.62 ± 0.49	Galaxy

Notes. Star 3778 (HD36861 C) is located about 30″ south of the star λ Orionis. This F8 V star is a member of the central multiple system of the cluster (Lindroos 1985; Bouy et al. 2009). Its strong infrared excess at 8 μm and 24 μm suggests that 3778 is an intermediate-mass star surrounded by an optically thick disk. Star 1959 (NLTT15297) is a double system reported as a high proper motion star. Its optical colors reported in SIMBAD suggests that 1959 is a foreground system. This star does not have photometry in the optical database used in Section 3.2. Star 5968 is the only possible diskbearing star with discrepant photometric membership in Section 3.2 (see the text). Star 4244 is the faintest object with excess at 24 μm. Since this object does not exhibit excess at 8 μm, 4244 could be a transitional disk around a very low mass object in the λ Orionis cluster. Additional observations are required to confirm membership for this object.

REFERENCES

Backman, D. E., & Paresce, F. 1993, in Protostars and Planets III, ed. E. H. Levy & J. I. Lunine (Tucson, AZ: Univ. Arizona Press), 1253

Bally, J. 2008, in Handbook of Star Forming Regions, Volume I: The Northern Sky ASP Monograph Publications, ed. B. Reipurth (San Francisco, CA: ASP), 459

Barrado y Navascués, D., Stauffer, J. R., Bouvier, J., Jayawardhana, R., & Cuillandre, J.-C. 2004, ApJ, 610, 1064

Barrado y Navascués, D., Stauffer, J. R., Morales-Calderón, M., & Bayo, A. 2007a, RevMexAA Conf. Ser., 29, 37

Barrado y Navascués, D., et al. 2007b, ApJ, 664, 481 (BN07)

Bouy, H., et al. 2009, A&A, 504, 199

Briceño, C., Hartmann, L., Hernández, J., Calvet, N., Vivas, A. K., Furesz, G., & Szentgyorgyi, A. 2007, ApJ, 661, 1119

Brown, J. M., Blake, G. A., Qi, C., Dullemond, C. P., & Wilner, D. J. 2008, ApJ, 675, L109

Calvet, N., D'Alessio, P., Hartmann, L., Wilner, D., Walsh, A., & Sitko, M. 2002, ApJ, 568, 1008

Calvet, N., et al. 2005, ApJ, 630, L185

Carpenter, J. M. 2001, AJ, 121, 2851

Carpenter, J. M., Mamajek, E. E., Hillenbrand, L. A., & Meyer, M. R. 2006, ApJ, 651, L49

Cieza, L. A. 2008, in ASP Conf. Ser. 393, New Horizons in Astronomy, ed. A. Frebel et al. (San Francisco, CA: ASP), 35

Cunha, K., & Smith, V. V. 1996, A&A, 309, 892

Currie, T. 2010, arXiv:1002.1715

Currie, T., Kenyon, S. J., Balog, Z., Rieke, G., Bragg, A., & Bromley, B. 2008, ApJ, 672, 558

Currie, T., Lada, C. J., Plavchan, P., Robitaille, T. P., Irwin, J., & Kenyon, S. J. 2009, ApJ, 698, 1

Dahm, S. E., & Hillenbrand, L. A. 2007, AJ, 133, 2072
D'Alessio, P., Calvet, N., Hartmann, L., Franco-Hernández, R., & Servín, H. 2006, ApJ, 638, 314
D'Alessio, P., et al. 2005, ApJ, 621, 461
Dame, T. M., Hartmann, D., & Thaddeus, P. 2001, ApJ, 547, 792
Diplas, A., & Savage, B. D. 1994, ApJS, 93, 211
Dolan, C. J., & Mathieu, R. D. 1999, AJ, 118, 2409
Dolan, C. J., & Mathieu, R. D. 2001, AJ, 121, 2124
Dolan, C. J., & Mathieu, R. D. 2002, AJ, 123, 387 (DM02)
Duerr, R., Imhoff, C. L., & Lada, C. J. 1982, ApJ, 261, 135
Dullemond, C. P., & Dominik, C. 2005, A&A, 434, 971
Dullemond, C. P., Hollenbach, D., Kamp, I., & D'Alessio, P. 2007, in Protostars and Planets V, ed. B. Reipurth, D. Jewitt, & K. Keil (Tucson, AZ: Univ. Arizona Press), 555
Engelbracht, C. W., et al. 2007, PASP, 119, 994
Ercolano, B., Clarke, C. J., & Robitaille, T. P. 2009, MNRAS, 394, L141
Espaillat, C., Calvet, N., Luhman, K. L., Muzerolle, J., & D'Alessio, P. 2008a, ApJ, 682, L125
Espaillat, C., et al. 2007a, ApJ, 664, L111
Espaillat, C., et al. 2007b, ApJ, 670, L135
Espaillat, C., et al. 2008b, ApJ, 689, L145
Fazio, G. G., et al. 2004, ApJS, 154, 39
Furlan, E., et al. 2006, ApJS, 165, 568
Furlan, E., et al. 2009, ApJ, 703, 1964
Gorlova, N., Balog, Z., Rieke, G. H., Muzerolle, J., Su, K. Y. L., Ivanov, V. D., & Young, E. T. 2007, ApJ, 670, 516
Gorlova, N., Rieke, G. H., Muzerolle, J., Stauffer, J. R., Siegler, N., Young, E. T., & Stansberry, J. H. 2006, ApJ, 649, 1028
Greenberg, R., et al. 1978, Icarus, 35, 1
Haisch, K. E., Lada, E. A., & Lada, C. J. 2001, ApJ, 553, L153
Hartmann, L., Megeath, S. T., Allen, L., Luhman, K., Calvet, N., D'Alessio, P., Franco-Hernandez, R., & Fazio, G. 2005, ApJ, 629, 881
Hernández, J., Briceño, C., Calvet, N., Hartmann, L., Muzerolle, J., & Quintero, A. 2006, ApJ, 652, 472
Hernández, J., Calvet, N., Hartmann, L., Muzerolle, J., Gutermuth, R., & Stauffer, J. 2009, ApJ, 707, 705 (Paper I)
Hernández, J., Hartmann, L., Calvet, N., Jeffries, R. D., Gutermuth, R., Muzerolle, J., & Stauffer, J. 2008, ApJ, 686, 1195
Hernández, J., et al. 2007a, ApJ, 662, 1067
Hernández, J., et al. 2007b, ApJ, 671, 1784
Hillenbrand, L. A. 2005, arXiv:astro-ph/0511083
Hillenbrand, L. A. 2008, Phys. Scr. T, 130, 014024
Ireland, M. J., & Kraus, A. L. 2008, ApJ, 678, L59
Kenyon, S. J., & Bromley, B. C. 2004, AJ, 127, 513
Kenyon, S. J., & Bromley, B. C. 2005, AJ, 130, 269
Kenyon, S. J., & Bromley, B. C. 2008, ApJS, 179, 451
Kenyon, S. J., & Hartmann, L. 1987, ApJ, 323, 714
Kenyon, S. J., & Hartmann, L. 1995, ApJS, 101, 117
Kharchenko, N. V., & Roeser, S. 2009, VizieR Online Data Catalog, 1280, 0
Lada, C. J., et al. 2006, AJ, 131, 1574
Landsman, W. B. 1993, in ASP Conf. Ser. 52, Astronomical Data Analysis Software and Systems II, ed. R. J. Hanisch, R. J. V. Brissenden, & J. Barnes (San Francisco, CA: ASP), 246
Lindroos, K. P. 1985, A&AS, 60, 183
Luhman, K. L., Allen, P. R., Espaillat, C., Hartmann, L., & Calvet, N. 2010, ApJS, 186, 111
Luhman, K. L., Hernández, J., Downes, J. J., Hartmann, L., & Briceño, C. 2008, ApJ, 688, 362
Maddalena, R. J., & Morris, M. 1987, ApJ, 323, 179
Manoj, P. 2010, arXiv:1003.5933
Mathieu, R. D. 2008, in Handbook of Star Forming Regions, Volume I: The Northern Sky ASP Monograph Publications, ed. B. Reipurth (San Francisco, CA: ASP), 757
Maxted, P. F. L., Jeffries, R. D., Oliveira, J. M., Naylor, T., & Jackson, R. J. 2008, MNRAS, 385, 2210
Morales-Calderon, M. 2009, PhD thesis, Univ. Autónoma Madrid
Murdin, P., & Penston, M. V. 1977, MNRAS, 181, 657
Muzerolle, J., Allen, L. E., Megeath, S. T., Hernández, J., & Gutermuth, R. A. 2010, ApJ, 708, 1107
Pasquini, L., et al. 2002, The Messenger, 110, 1
Podosek, F. A., & Cassen, P. 1994, Meteoritics, 29, 6
Rieke, G. H., et al. 2004, ApJS, 154, 25
Sacco, G. G., Franciosini, E., Randich, S., & Pallavicini, R. 2008, A&A, 488, 167
Schlegel, D. J., Finkbeiner, D. P., & Davis, M. 1998, ApJ, 500, 525
Sicilia-Aguilar, A., Henning, T., Juhász, A., Bouwman, J., Garmire, G., & Garmire, A. 2008, ApJ, 687, 1145
Siess, L., Dufour, E., & Forestini, M. 2000, A&A, 358, 593
Skrutskie, M. F., et al. 2006, AJ, 131, 1163
Tobin, J. J., Hartmann, L., Furesz, G., Mateo, M., & Megeath, S. T. 2009, ApJ, 697, 1103
Werner, M. W., et al. 2004, ApJS, 154, 1
Wyatt, M. C. 2008, ARA&A, 46, 339
Zhang, C. Y., Laureijs, R. J., Chlewicki, G., Wesselius, P. R., & Clark, F. O. 1989, A&A, 218, 231